604084

Insights into Corona Formation through Statistical Analyses

LS Glaze[1], ER Stofan[1], SE Smrekar[2] and SM Baloga[1]
[1] Proxemy Research, 20528 Farcroft Lane, Laytonsville, MD 20882
[2] Jet Propulsion Laboratory, 4800 Oak Grove Drive, Pasadena, CA 91109

Submitted to JGR/Planets: March 8, 2002; Revised: June 21, 2002

Abstract: Statistical analysis of an expanded database of coronae on Venus indicates that the populations of Type 1 (with fracture annuli) and 2 (without fracture annuli) corona diameters are statistically indistinguishable, and therefore we have no basis for assuming different formation mechanisms. Analysis of the topography and diameters of coronae shows that coronae that are depressions, rimmed depressions, and domes tend to be significantly smaller than those that are plateaus, rimmed plateaus, or domes with surrounding rims. This is consistent with the model of Smrekar and Stofan [1997] and inconsistent with predictions of the spreading drop model of Koch and Manga [1996]. The diameter range for domes, the initial stage of corona formation, provides a broad constraint on the buoyancy of corona-forming plumes. Coronae are only slightly more likely to be topographically raised than depressions, with Type 1 coronae most frequently occuring as rimmed depressions and Type 2 coronae most frequently occuring with flat interiors and raised rims. Most Type 1 coronae are located along chasmata systems or fracture belts, while Type 2 coronae are found predominantly as isolated features in the plains. Coronae at hotspot rises tend to be significantly larger than coronae in other settings, consistent with a hotter upper mantle at hotspot rises and their active state.

Introduction

Coronae are circular to elliptical features on Venus (Figure 1) with diameters of approximately 100 to over 1000 km, that have been suggested to form over thermal upwellings [Stofan et al., 1991; Janes et al., 1992; Koch and Manga, 1996; Musser and Squyres, 1997; Smrekar and Stofan, 1997]. Coronae have a range of topographic forms, including plateaus, plateaus with raised rims, and rimmed depressions [Smrekar and Stofan, 1997; Stofan et al., 2001]. Most coronae are also associated with volcanic features, including edifices and flow fields in their interiors and exterior flows [Squyres et al., 1992; Stofan et al., 1992].

Recently, the population of coronae was split into two types: Type 1 coronae, that have annuli of concentric ridges and/or fractures; and Type 2 coronae, that have similar characteristics to Type 1 coronae but lack a complete annulus of ridges and fractures [Stofan et al., 2001]. A survey of Magellan image and topographic data resulted in the identification of 406 Type 1 coronae and 107 Type 2 coronae (http://webgis.wr.usgs.gov/venus_general.htm). Stofan et al. [2001] found in an initial analysis of the expanded population that Type 2 coronae have a smaller mean diameter, tend to have relatively flat interiors surrounded by a topographic rim, and are more likely to be found in settings isolated from other types of geologic features.

The updated corona database [Stofan et al., 2001] presents a unique opportunity to perform rigorous statistical analyses. The database contains a large amount of data that come from a remarkably well-defined population. Here we have the ability, not only to perform a wide variety of statistical hypothesis tests, but also validate the underlying statistical assumptions of those tests.

The goal of the statistical analysis presented here is to determine which properties of the coronae are statistically uniform and which, if any, are different. There are a variety of factors that could be used to group coronae, e.g., Type 1 vs. Type 2, diameter, geologic setting, or topographic characteristics. Variability in these characteristics may indicate the influence of factors such as age, thickness of the lithosphere, variations in plume size, or overall formation processes. Competing corona formation processes have been suggested in the literature, such as the model for deformation of the surface by upwellings [Stofan et al., 1991; Janes et al., 1992; Cyr and Melosh, 1993; Musser and Squyres, 1997], the delamination model of Smrekar and Stofan [1997], and the spreading drop model of Koch and Manga [1996]. Each of these models make predictions about factors such as the relationship between diameter and topographic morphology. Statistical analysis of corona population and subpopulation differences may support one process model versus the other and substantiate the need for further refinements of such models.

Attachment A

Stofan et al. [2001] interpreted the Type 2 coronae to have formed by the same process as Type 1 coronae based on their general similarities in topographic characteristics, overall size range, and association with volcanism. However, no rigorous tests were performed to support this hypothesis. In this study, we focus on the diameter of Type 1 and Type 2 features and their distinctive topographic signatures to determine if the two types of coronae are likely to come from the same population. The diameters of coronae are easily measured and are one way of characterizing each feature. For now, the diameters are the only quantitative data we have available for analysis. If the distributions of corona diameters are statistically indistinguishable, we cannot preclude the possibility that the Type 1 and Type 2 coronae were formed by the same basic process. Furthermore, until additional data (e.g., gravity, or other corona dimensions) show statistically signficant differences between the corona types, we have no basis for assuming different formation processes. Here, we analyze the relationship between diameter and topographic group, both in terms of assessing the relationship between Type 1 and Type 2 coronae as well as model predictions for corona formation. We also evaluate how diameter and topographic group relate to the geologic settings of the coronae.

Coronae Data Base

The 406 Type 1 coronae analyzed in this study include most of the original population of 360 coronae identified by Stofan et al. [1992], along with additional features that have been identified through further analysis of the Magellan data [Stofan et al., 2001]. Some features from the original population were also reclassified as Type 2 coronae. The number of features used here differs from that presented in Stofan et al. [2001], due to the reclassification of Isong Corona (12°N, 49.2°) from a Type 1 corona to a Type 2 corona, and the deletion of a duplicate entry. Type 1 coronae were identified visually in Venera 15/16 and Magellan SAR (synthetic aperture radar) image data, primarily based on their distinctive annuli of concentric ridges and/or fractures [e.g., Basilevsky et al., 1986; Squyres et al., 1992]. The diameters (or maximum widths for non-circular coronae) were determined by measuring to the outermost extent of concentric deformation. The smallest feature identified was 60 km across, and the largest was Artemis Corona, with a diameter of 2600 km. The next largest corona is Heng-o, with a diameter of 1060 km. In the analyses described here, we did not include Artemis in the Type 1 population, as it is clearly an outlier, and may have formed by a different set of processes [Sandwell and Schubert, 1992; Brown and Grimm, 1995].

The 107 Type 2 coronae have less than 180° of fracture annulus, including many features that completely lack a fracture annulus [Stofan et al., 2001]. Type 2 coronae were originally called 'stealth coronae' [Tapper, 1997], as not all of them can be identified using only Magellan SAR (synthetic aperture radar) images. Instead these features were identified primarily by their topographic signatures. Maximum widths were determined by measuring between the outermost breaks in slope. At Type 1 coronae, the fracture annulus can occur at differnet locations with respect to the raised rim (inside, outside, or coincident). Therefore, we do not expect any systematic differences to result from the two methods of measuring maximum width. Further, we do not interpret the fracture annulus at Type 2 coronae that have partial fracture rims to simply have been covered by volcanic flooding [Stofan et al., 2001]. As the fracture annuli at both Type 1 and 2 coronae most commonly occur on a raised topographic rim, the annuli are not more vulnerable to burial than the rims.

Statistical Analyses

The primary objective of this study is to ascertain if the coronae are all part of a single population based on their diameter, and if there are statistically distinguishable subpopulations based on secondary factors, such as type, geologic setting, or topography. Statistical inferences cannot be used to "prove" such hypotheses. However, in statistical language, we can accept hypotheses that are not strictly "precluded". In order to infer that two samples come from the same population they must be statistically indistinguishable, i.e., they must each exhibit the same sampling distribution (e.g., normal, lognormal, etc.). In addition to general shape, the two samples should have similar values for the parameters of the distribution. The most common parameters for characterizing a distribution are the mean value, standard deviation, skewness and kurtosis. If the shape of the distributions, and the statistical parameters are indistinguishable, then we have no reason to suspect different formative processes based on the data alone. Conversely, if they are different, we are encouraged to look beyond the statistics into different physical processes or geologic parameters for some plausible explanation. The remainder of this section contains descriptions of rigorous hypothesis tests conducted on a variety of combinations of the data contained in the coronae database. For all hypothesis tests conducted here, we have assumed a significance level of 5% ($\alpha = 0.05$). The implication

of this assumption is that there is a 5% probability of accepting our hypothesis when, in fact, it should be rejected.

Type 1 Coronae vs. Type 2 Coronae

We would like to test whether or not the diameters of the two broad groups of coronae, Type 1 and Type 2, come from the same population. The motivation for this comparison is to assess whether the only difference between these two types of coronae is the existence of, or lack of, surface fractures. However, before such statistical comparisons can be made, we must first determine the probability distributions that best describe the two data sets. Summary statistics for Type 1 and 2 coronae are given in Table 1 and frequency histograms of the diameters are shown in Figure 2.

Upon visual inspection of the distributions of Type 1 and 2 coronae diameters in Figure 2, both appear to be strongly asymmetric and very peaked. Skewness is a statistical measure of the asymmetry of a distribution and kurtosis is a measure of its peakedness. The so-called standardized forms of these statistics are often used to facilitate an immediate evaluation of their significance. The standardized skewness and kurtosis (as determined by Statgraphics Plus ™, v4.0) for both data sets is greater than 2 (see Table 1), indicating significant deviation from the normal (Gaussian) distribution. Most standard hypothesis tests assume data that are normally distributed. It is clear that this common assumption is violated for the corona data.

The lognormal distribution is the natural choice for describing asymmetric distributions of geologic data such as the corona diameters. Some authors [e.g., Bowen and Bennett, 1988; Johnson et al., 1994] consider this distribution as important as the normal distribution based on its wide variety of applications. Such distributions arise when random effects are multiplicative in a natural process, effects occur on multiple scales, or there are mixtures of subpopulations. For comparison, the lognormal distribution is also plotted in Figure 2 along with the frequency histogram for each data set. Visually, the lognormal seems to agree quite well with the data.

To confirm that these data are lognormally distributed, we have conducted a rigorous χ^2 test to determine the goodness of fit. For the Type 1 coronae we have chosen to use 10 bins to best represent the 'shape' of the distribution. For 10 bins, the calculated χ^2 statistic is U = 6.04. To determine the goodness of fit, we compare this value with the critical value from the χ^2 distribution. The χ^2 distribution is described by a single parameter, the degrees of freedom. For this test, the degrees of freedom are found by subtracting 3 (1 each for the lognormal parameters, mean and standard deviation, plus 1 more for the χ^2 degrees of freedom parameter) from the number of bins used. The critical value is then found from the cumulative probability for the χ^2 distribution with 7 degrees of freedom. For our significance level of $\alpha = 0.05$, the critical value is the location at which the cumulative probability equals 95%, equal to 14.07. The fact that our statistic, U, is significantly less than the critical value strongly supports the use of the lognormal to describe Type 1 corona diameters.

Because the χ^2 distribution fitting hypothesis test may be sensitive to the number of bins that are used to perform the test, we have also looked at other bin sizes. For all reasonable choices of bins, the test strongly supports our hypothesis that the Type 1 corona diameters are lognormally distributed.

We have conducted the same χ^2 goodness of fit test for the Type 2 corona diameters. In this case we have chosen 8 bins due to the smaller number of data points contained in this data set (107 as opposed to 406). For 8 bins, the χ^2 statistic U = 3.58. The critical value from the χ^2 distribution is 11.1 for α = .05 and 5 degrees of freedom. Therefore, the Type 2 diameters are also very strongly lognormal. Again, slight changes in the number of bins does not affect our conclusion regarding the lognormal nature of the data.

Now that we have determined that both data sets are lognormal in character, we can proceed to compare the mean values and standard deviations in order to ascertain whether significant differences exist between the two populations. As stated earlier, most hypothesis tests assume that the sample populations are normally distributed. Fortunately, because the data are lognormally distributed, we can easily transform the corona data such that they are normal by taking the natural log of the diameters. We have, therefore, transformed both data sets, conducted the tests, and then transformed the results back into original units by exponentiation.

The arithmetic mean value of the transformed data is identically the geometric mean value of the untransformed data. Thus, our results are given with respect to the geometric mean. Note that, in general, the geometric mean is more appropriate than the arithmetic mean for asymmetric distributions with long tails, such as the corona diameters. This is because the small number of large values in the tail increases the arithmetic mean such that it does not adequately characterize the central tendency of the data.

The Type 1 coronae have a geometric mean diameter of 220.7 km with a corresponding 95% confidence interval of 210.0 – 234.6 km. The Type 2

coronae have a geometric mean diameter of 208.0 km with a corresponding 95% confidence interval of 188.5 – 229.6 km. Figure 3 illustrates the geometric mean values for the Type 1 and 2 coronae along with their associated confidence intervals. There is a reasonable amount of overlap between these two confidence intervals indicating that the two mean values cannot be distinguished statistically.

Similarly, we have examined the standard deviations by conducting an F-test on the transformed data. The F-test is the conventional method for comparing standard deviations. The standard deviations for the transformed Type 1 and 2 diameters are 0.56 and 0.51, respectively. The test statistic for comparing two standard deviations is simply $s_{T1}^2/s_{T2}^2 = 1.20$. The ratio of variances (standard deviation squared) has an F distribution that is described by two parameters. Our estimates of these two parameters, the degrees of freedom, are found by subtracting 1 from the total number of data points in each of the data sets being tested. It should be noted that this is a two-tailed test and that for a significance level of 5%, the critical value of the F distribution is found at a cumulative probability of 0.975 [see discussion in Sheskin, 1997]. The critical value for testing whether the two standard deviations are the same with a 5% significance level is 1.373, for (405,106) degrees of freedom. The value of our test statistic is below the critical value indicating that, again, the two standard deviations are statistically indistinguishable.

From the tests conducted above, we have concluded that the Type 1 and 2 coronae diameters are both distributed lognormally. More importantly, both lognormal sampling distributions have the same shape and parameters. Thus, based on the distribution of corona diameters alone, there is no evidence to suggest the possibility of different formative processes for Type 1 and Type 2 coronae.

Topographic Subgroup Comparisons

Type 1 and 2 coronae have been classified into nine topographic groups, with group 3 having two subcategories: 1) domes; 2) plateaus; 3a) rimmed plateau; 3b) rim surrounding an interior topographic high; 4) rim surrounding depressions; 5) outer rise, trough, interior high; 6) outer rise, trough, rim, interior depression; 7) rim only; 8) depressions; and 9) no discernible topographic signature [Smrekar and Stofan, 1997; Stofan et al., 2001]. As seen in Table 2, group 4 (rimmed depressions) is the most commonly occurring Type 1 corona. Group 3b (rim surrounding raised interiors) follows group 4 with just over half as many coronae. In contrast (see Table 3), Type 2 coronae are dominated by topographic groups 7 (rim only) and 4, with 7 containing over twice as many coronae as 4. Combining the Type 1 and 2 coronae, topographic group 4 is by far the most commonly occurring corona on Venus. Figure 4 shows these relationships graphically.

While overall the Type 2 coronae do not appear to be fundamentally different than the Type 1 coronae, the lognormal distribution is sometimes indicative of multiple processes occurring at different scales. Because the database already contains logical subclassifications according to topographic subgroup and geologic setting, we can begin by comparing the distributions of diameters between these groups. Of course, there will always be some features that are ambiguous as to which topographic group they belong, or perhaps even whether or not they are Type 1 or 2. This is precisely why we use statistics to quantify our uncertainty and to help us distinguish differences between subpopulations. Our objective is to determine if there are any factors that sets one or more of these subgroups apart from the others.

As with the analyses discussed above, we must determine the probability distributions that best describe each of the topographic groups before statistical comparisons can be made. Again, the subgroup data are all non-normal in character; however, hypothesis tests can still be performed by using appropriate data transformations. We would like to combine the Type 1 and Type 2 data for each subgroup. Unfortunately, only topographic groups 4 and 7 contain enough Type 2 features to perform a meaningful comparison to Type 1.

Figure 5 shows Type 1 and 2 diameter data for subgroups 4 and 7 where the data have been transformed by taking the natural log. This transformation results in roughly normal distributions for all four subgroups. To test whether or not the normal distribution is appropriate for the transformed data, we conducted a set of rigorous χ^2, goodness of fit tests on each subgroup for $\alpha = .05$. Because the results of the χ^2 hypothesis test may be dependent upon binsize [Sheskin, 1997], we have taken into consideration a variety of approaches to optimal binning [Scott, 1979, Sheskin, 1997] to determine our "best estimate" for the number of bins, keeping in mind that there is no way to know the "correct" number of bins. Tables 2 and 3 indicate whether or not the normal distribution can be accepted or rejected for each choice of binsize (all subgroups but 6 have been tested for Type 1 coronae). The third column in the tables indicates our best estimate of the optimal number of bins for assessing the normality of the distribution. The fourth column indicates the χ^2 results for the optimal number of bins, and the last two columns give an indication of the sensitivity of our conclusions to the number of bins used in the

χ^2 test. Subgroups not assessed in the tables are too sparsely populated to conduct meaningful distribution fits (i.e., no distribution can be precluded). For every subgroup tested, at least one choice of binsize resulted in acceptance of the normal distribution. From these tests, we conclude that the normal distribution cannot be precluded for any of the individual transformed data sets.

Figure 6 compares the geometric mean values for subgroups 4 and 7, along with corresponding 95% confidence intervals. It can be seen that there is significant overlap in both cases. Based on this simple analysis, we will proceed under the assumption that the Type 1 and Type 2 corona diameters within individual subgroups are statistically indistinguishable. The Type 1 and 2 coronae are, therefore, combined for the remainder of this analysis. Figure 7 shows the combined transformed diameters for each topographic subgroup. We are now able to compare the individual subgroups for statistical differences.

In general, the group of inferential statistical procedures employed to evaluate whether or not there is a difference between more than two mean values are called analysis of variance (or ANOVA in the statistical literature). Within the confines of ANOVA, there are a variety of hypothesis tests that can be called upon to test the significance of differences between the mean diameter values of the topographic subgroups. Three such tests are Fisher's least significant difference (LSD), Bonferroni-Dunn and Scheffé [Sheskin, 1997]. Each test has its strengths and weaknesses. If we think in terms of confidence intervals, these tests will generate an interval around the mean diameter value for each subgroup and then evaluate the degree of overlap between the intervals. These confidence intervals take into account the reduced degrees of freedom resulting from the simultaneous estimation of means and standard deviations for multiple data sets. The magnitudes of the intervals generated by each approach vary somewhat due to constraints on the significance levels for the tests.

In broad terms, Fisher's LSD intervals are the tightest (or smallest). This means that this test is the most powerful for being able to distinguish between statistically different populations. With this test, the risk of concluding two means are the same, when in fact they are not (a Type II error in statistics, unrelated to Type 2 coronae), is reduced. However, this approach simultaneously increases the possibility of rejecting the overlap of two means when in truth they may be the same. At the other end of the spectrum, Scheffé intervals are larger in magnitude than the LSD intervals. This means that there is greater possibility for overlap between subgroups. Of course, simultaneously, the chance of accepting the overlap of two means, when in truth they are different, also increases. The magnitude of the Bonferroni-Dunn intervals generally fall somewhere between the LSD and Scheffé.

The approach we have taken to compare the subgroups is to calculate the 95% intervals by all three approaches described above. We have excluded topographic group 6 (outer rises surrounding troughs and inner lows) from comparative analysis because it is too sparsely populated. For the actual ANOVA, we have used the transformed data.

Table 4 illustrates the overlap in the confidence intervals around the mean diameters between subgroups for all three tests. Fortunately, the results of all three tests are consistent with each other. Figure 8 shows the geometric mean values and 95% Bonferroni intervals for each group, in the original units (km). We can see that there is substantial overlap between some groups, and none between others. From Table 4 we see that the LSD results strongly support the same conclusions as the Bonferroni. Even with the conservative Scheffé intervals, there is no overlap between subgroups 1, 4, 8 and 9 with 3a, 3b and 5.

From these analyses, we conclude that coronae that are rimmed depressions, depressions and domes (groups 4, 8 and 1) tend to be significantly smaller. Coronae that are plateaus, rimmed plateaus, or have rims surrounding central domes (groups 2, 3a, 3b and 5) tend to be larger. With the exception of domes (group 1), all the topographic groups with raised interiors are systematically larger.

Geologic Setting Comparisons

All coronae have also been classified according to the geologic setting in which they occur. Coronae occur predominantly in three geologic settings: along chasmata or fracture belts (group F), at hotspot rises (R) and as isolated features in the plains (P). Of the 513 combined Type 1 and 2 coronae, 3 occur on Lakshmi Planum (a volcanic highland plateau), and only 5 in the tessera. All 8 of these coronae are Type 1. As they are rare, coronae in these settings have not been included in the following analyses.

Of the remaining 505 coronae, 62% occur along fracture belts, 25% are isolated in the plains, and 11% are found at rises. Figure 9a shows the distribution of all coronae according to both topographic group and geologic setting. From this figure, we can see that for all topographic groups except 7, most coronae are found along chasmata (F). Group 7 coronae, however, are preferentially found isolated from other types of geologic features in the plains (P). Figure 9b illustrates the distribution of coronae found along chasmata and at hotspot rises in a slightly different

way. Here, the frequencies of occurrence for the topographic groups are shown as percentages of all coronae found in each setting. With the data presented in this way, we can see that Group 4 coronae occur more frequently along chasmata than at hotspot rises, with plateaus (2) and rimmed plateaus (3a) slightly more common at hotspot rises.

We can also break down this analysis further to examine the frequency of occurrence for the Type 1 and 2 coronae individually. From Figure 10a we can see that the distribution of Type 1 coronae is very similar to the combined distribution owing to the large number of features. The primary differences between Figures 9a and 10a are in topographic groups 4 and 7, where most of the Type 2 coronae occur. Figure 10b shows the distribution of Type 2 coronae. Here we can clearly see the apparent preference of the Type 2 coronae to form in the plains as opposed to along chasmata, not only for topographic group 7, but for group 4 as well.

Just as we did for the topographic groups, we can also look for fundamental differences between the diameters of coronae found in the three most populated geologic settings. For this comparison, we have combined the Type 1 and 2 coronae and calculated the 95% LSD, Bonferroni, and Scheffé intervals around the geometric mean value for each subgroup. Figure 11 shows the mean values and associated Bonferroni confidence intervals for the three geologic setting subgroups. Regardless of whether LSD, Bonferroni or Scheffé intervals are used, the conclusions are the same. There is convincing overlap between the F and P subgroups, while the hotspot rise coronae are systematically larger.

Discussion

Coronae were originally identified as commonly having raised topography (e.g., Basilevsky et al., 1986; Pronin and Stofan, 1990). However, it can be seen from Tables 2 and 3 that the 184 coronae that are depressions (Groups 4, 6, and 8) are similar in number to the 226 that are topographically raised (Groups 1, 2, 3a, 3b and 5). A hypothesis test of binomial proportions with $\alpha = .05$ indicates that, for 410 coronae (excluding Topographic Groups 9 – no topographic signature, and 7 – neither raised nor depressed), an interval of equal probability can be defined between 185 and 225. Because the numbers of raised and depressed coronae are just outside the interval, this implies a slight deviation from an equal probability (50/50) of occurrence. One can easily argue that coronae that are depressions may be just as likely to occur on Venus as those that are raised.

The abundant volcanism associated with coronae, as well as the assumption of raised topography, led most workers to utilize models of origin associated with thermal upwelling [Stofan et al., 1991; Janes et al., 1992; Koch and Manga, 1996; Musser and Squyres, 1997; Smrekar and Stofan, 1997]. However, the greater abundance of coronae with flat or low interiors puts even greater emphasis on the need for fully understanding how all topographic expressions are produced. Downwelling models were originally assessed and rejected by Stofan et al. [1991] due to difficulties in producing the observed volcanism and extensional deformation. Upwelling models can produce topographic depressions if there is significant crustal thinning [Koch and Manga, 1996], thinning of a depleted mantle layer [Smrekar and Parmentier, 1996; Smrekar and Stofan, 1997], or active delamination, initiated by viscous coupling of the cold lower lithosphere to flow at the margins of a plume head [Smrekar and Stofan, 1997].

All models of upwelling plumes are consistent with an increase in size from the initial dome created above a plume head to plateau due to spreading of the plume head under the lithosphere. Beyond this phase, the two models that predict both raised and depressed topography, Koch and Manga [1996] and Smrekar and Stofan [1997], make quite different predictions about the predicted size of coronae. Analyses of the corona diameters conducted here can be compared to the predicted size progressions of these models to determine which model provides a better fit to the observations.

The data indicate that coronae with domes, depressions, and rimmed depressions are smaller than those that are plateaus, rimmed plateaus, and rims surrounding central topographic highs. The spreading drop model of Koch and Manga [1996] predicts that, for a given crustal thickness, diameters become progressively larger as coronae progress from dome to plateau to rim only to rimmed depression. For a given example representative of typical corona diameters, the dome stage is a little larger than half the diameter of the final rimmed depression stage [Koch and Manga, 1996]. Clearly this progression of sizes is not apparent in the data. Nor is the expected trend seen when one normalizes for variations in crustal thickness [Smrekar and Stofan, 2002].

The observation that domes and topographic forms with flat or depressed interiors are significantly smaller than plateaus with a wide range of variations is consistent with model predictions of Smrekar and Stofan [1997]. Depressions are formed in one of two ways. By the first mechanism, depleted mantle is thinned over a rising plume, producing a depression approximately the same size as the dome that would

be produced in the absence of a low density depleted mantle layer. Thinning of a low density depleted mantle layer produces a depression as the density of the overall lithospheric column is reduced [Smrekar and Parmentier, 1996]. In the second mechanism, viscous coupling between the cold, dense, lower lithosphere and the edge of the plume head initiates delamination. The delaminating lower lithosphere forms a ring that migrates in to the center of the corona, causing an interior depression similar in size to the original dome [see Figure 3., Smrekar and Stofan, 1997]. If a depleted mantle layer is present, isostatic rebound of the thickened depleted mantle layer occurs once the delamination ceases due to thermal equilibration of the cold lower lithosphere. This isostatic rebound produces a rim only corona. This topographic form could also be produced by isostatic rebound of a thickened crustal layer. Rim only coronae can be larger than coronae actively undergoing delamination because the balance of forces changes as delamination ceases, allowing minor outward migration of the isostatically rebounding ring. Analysis of the gravity signature of numerous Type 2 rim only coronae confirms the importance of compensation due to a density interface, most likely a crustal layer [Smrekar and Stofan, 2002].

All corona models indicate that domes are the first stage of evolution. When there is no plate motion, the dome radius and height are a function of the initial plume buoyancy and the viscosity contrast between the plume and surrounding upper mantle [Olsen and Nam, 1986; Musser and Squyres, 1997; Ribe and Christensen, 1999]. The plume buoyancy is the product of the plume size and density contrast due to thermal and any chemical variations between the plume and the surrounding mantle. The viscosity contrast primarily controls the degree of spreading of the plume head under the lithosphere [Musser and Squyres, 1997]. Thus for domes, where little spreading has occurred, the plume buoyancy should be the dominant variable. Variations in the thickness of the lithosphere primarily affect the axial height of the topographic swell and the degree of melting, and have only a secondary influence on the radius of the swell [e.g. Olsen and Nam, 1986; Smrekar and Parmentier, 1996].

Thus we can use the statistics on dome diameters to provide a general constraint on the range of plume buoyancy and viscosity contrast. Using the natural log transformation appropriate for a lognormal distribution, we find that 95% of domes have a diameter in the range of 69 - 461 km. The work of Olsen and Nam [1986], which uses a combination of laboratory experiments and analytic equations to parameterize the behavior of rising blobs, focuses on the initial uplift phase of the swell deformation and is perhaps the most applicable to the formation of corona domes. For a given mantle viscosity and plume density contrast, Olsen and Nam [1986] find that the initial plume size is directly proportional to the dome diameter. Thus the range of a factor of 6 - 7 in dome diameter reflects a similar range in the plume buoyancy, and could reflect variations in the size, density contrast, or both in the initial plumes that form coronae. Uniform upper mantle viscosity is probably a reasonable assumption, and density contrast and size can be interchanged. Musser and Squyres [1997] estimated a more limited range of initial plume variation, a factor of 3, based on considering the range of concentric corona diameters and including the effects of the plume head spreading. The strength of the statistical analysis of a larger group of coronae and the focus on domes alone should produce a more accurate number. This value could be further refined by considering the dome heights and estimating their compensation state to determine if they are actively supported by plumes.

Coronae in Topographic Group 9, those with no distinct topographic signature, are significantly smaller than plateaus, rimmed plateaus and rims surrounding central domes. These features are likely amongst the oldest coronae, with any prior topography fully relaxed. Since they overlap in size with domes, rimmed depressions, rim only, and depressions, they may be very late stage forms of these coronae in which all topography has relaxed.

Additionally we have determined that there is statistically no difference between the mean and standard deviation of the diameters of Type 1 and Type 2 distributions. We interpret this result, along with strong similarities in topographic morphology and associated volcanism, to indicate that these coronae are likely to have formed by the same process or processes. However, the two types of coronae do have some variations with respect to their abundance in geologic settings and classes of topographic morphology, as well as in the completeness of their annuli of fractures (by definition). As discussed in Stofan et al. [2001], Type 1 coronae are found most frequently along fracture belts and chasmata. Type 2 coronae are more likely to be found in plains regions, and are more likely to be rim only coronae, consistent with a depleted mantle layer underlying the plains [Smrekar and Stofan, 1997; Stofan et al. 2001]. Most Type 2 coronae are rim only coronae, followed by rimmed depressions. Analysis of the gravity signature for Type 2 rim only coronae indicates that they are compensated by a density interface, such as a crustal or depleted mantle layer [Smrekar and Stofan, 2002].

Most Type 1 coronae are rimmed depressions, followed by rims surrounding interior domes.

The lack of an annulus at Type 2 coronae may result from: 1) a strong lithosphere and low stress at the surface or 2) slow bending of the surface resulting in a low strain rate [Stofan et al., 2001]. The gravity signature of Type 2 coronae indicates that they form on the full range of lithospheric thickness found on Venus, thus indicating that strength of the lithosphere is not likely to be the discriminating factor [Smrekar et al., 2002; Smrekar and Stofan, 2002]. The gravity signature of rim only coronae can be interpreted to indicate that rim only coronae are either isostatically compensated or undergoing isostatic rebound [Smrekar and Stofan, 2002]. This is most consistent with slow bending of the lithosphere in response to isostatic rebound [Smrekar and Stofan, 2002].

Coronae at hotspot rises occur more frequently as plateaus and rimmed plateaus. These shapes are indicative of the earlier stages of corona formation [Koch and Manga, 1996; Smrekar and Stofan, 1997], which is consistent with the fact that hotspot rises are still likely to be active [Smrekar, 1994; Stofan et al., 1995]. Coronae at hotspot rises also tend to be larger than coronae in the plains or along chasmata. Low values of elastic thickness have been derived at venusian hotspot rises [Smrekar, 1994; Phillips et al., 1997; Simons et al., 1997; Smrekar et al., 1997; Barnett et al., 2000]. This implies a higher thermal gradient in the lithosphere and hotter mantle below rises. The higher upper mantle temperature lowers the viscosity and allows plumes to spread farther under the lithosphere, producing larger coronae [Musser and Squyres, 1997; Ribe and Christensen, 1999].

Conclusions

The updated corona database provides us with the opportunity to perform detailed statistical analyses of diameters, geologic setting, and topographic factors. The underlying assumptions of all statistical tests applied in this paper have been rigorously verified. More importantly, we are able to use these analyses to characterize corona subpopulations, which in turn can then be used to support or refute models of corona origin. Here we have investigated the nature of the diameter distributions and their parameter values to determine which combinations of factors lead to distinct populations or subpopulations. Our analysis indicates that both Type 1 and 2 corona diameters can be described by a lognormal distribution with parameters that are statistically indistinguishable. While these two corona types are fundamentally different in appearance, there is no compelling reason to contemplate different formative processes. Indeed, it is legitimate to combine the data into a single population.

There are enough coronae to perform a similar analysis on topographic groups 4 and 7 (coronae that are rimmed depressions or coronae with flat interiors and raised rims, respectively) and to validate the lognormal distribution for the sub-populations. Simultaneous comparison of mean values between the topographic subgroups using ANOVA techniques shows that coronae that are depressions, rimmed depressions, and domes tend to be significantly smaller than those that are plateaus, rimmed plateaus, or domes with surrounding rims. The size distribution of corona within each topographic group provides a new constraint on models of corona formation. Specifically the distribution of diameters supports the delamination model of Smrekar and Stofan [1997] and counters the predictions of the spreading drop model of Koch and Manga [1996]. The diameter range for domes, which represent the initial stage of uplift, provides a general constraint on the buoyancy of corona-forming plumes.

Similarly, corona size classified by geologic settings were analyzed using simultaneous inference methods. Here it has been shown that coronae at hotspot rises are systematically larger than coronae in other settings. This is consistent with the thinner elastic lithosphere and hotter mantle at hotspot rises and their active state. Conversely, there is no size difference between coronae in plains and fracture belts, suggesting uniform upper mantle temperatures and viscosities between these two settings.

Coronae are slightly more likely to be topographically raised than depressions, with Type 1 coronae most likely to be rimmed depressions and Type 2 coronae most likely to have flat interiors and raised rims. Most Type 1 coronae are located along chasmata systems or fracture belts, while Type 2 coronae are found predominantly as isolated features in the plains. We are in the process of relating these differences to other corona variables, such as gravity signature.

This analysis provides a sound basis for pursuing further theoretical studies to explain significant differences in the data in terms of physical processes. It also encourages the collection of more detailed measurements of other variables (e.g., rim heights, widths, depression depths, elevations) that can be used to further refine our understanding of the differences between different types of coronae.

Acknowledgements

This work was funded by the NASA Planetary Geology and Geophysics Program (NASW-00013, NAG5-10530 and RTOP# 344-30-43-03). A

NASA/Presidential Early Career Award to ERS is gratefully acknowledged.

References

Barnett, D.N., F. Nimmo, and D. McKenzie, 2000, Flexure of Venusian lithosphere measured from residual topography and gravity, *Icarus*, **16**, 404-419.

Basilevsky, A.T., A.A. Pronin, L.B. Ronca, V.P. Kryuchkov, A.L. Sukhanov, and M.S. Markov, 1986, Styles of tectonic deformation on Venus: Analysis of Veneras 15 and 16 data, *J. Geophys. Res.*, **91**, 399-411.

Bowen, W.M. and C.A. Bennett, 1988, *Statistical methods for nuclear material management*. US Nuclear Regulatory Commission, NUREG/CR-4604, 1000pp.

Brown, C.D. and R.E. Grimm, 1995, Tectonics of Artemis Chasma: A venusian "plate" boundary. *Icarus* **117**, 219-249.

Cyr, K.E. and H.J. Melosh, 1993, Tectonic patterns and regional stresses near Venusian coronae, *Icarus*, **102**, 175-184.

Janes, D.M, S.W. Squyres, D.L. Bindschadler, G. Baer, G. Schubert, V.L. Sharpton and E.R. Stofan, 1992, Geophysical models for the formation and evolution of coronae on Venus, *J. Geophys. Res.*, **97**, 16,055-16,067.

Johnson, N.L., S. Kotz and N. Balakrishnan, 1994, *Continuous univariate distributions, Vol 1*. John Wiley, New York, 756 pp.

Koch, D.M., and M. Manga, 1996, Neutrally buoyant diapirs: A model for Venus coronae, *Geophys. Res. Lett.*, **23**, 22-228.

Musser, G.S., Jr., and S.W. Squyres, 1997, A coupled thermal-mechanical model for corona formation on Venus, *J. Geophys. Res.*, **102**, 6581-6595.

Olsen, P. and I.S. Nam, 1986, Formation of seafloor swells by mantle plumes, *J. Geophys. Res.*, **91**, 7181-7191.

Phillips, R. J., C.L. Johnson, S.J. Mackwell, P. Morgan, D.T. Sandwell, and M.T. Zuber, 1997, Lithospheric mechanics and dynamics of Venus. In *Venus II* (Bougher, S. W., D.M. Hunten, R.J. Phillips, eds.), Univ. of Arizona Press, Tucson, pp. 1163-1204.

Pronin, A.A., and E.R. Stofan, 1990, Coronae on Venus: Morphology and distribution, *Icarus*, **87**, 452-474.

Ribe, N.M. and U.R. Christensen, 1999, The dynamical origin of Hawaiian volcanism, *Earth Planet. Sci. Lett.*, **171**, 517-531.

Sandwell, D.T. and G. Schubert, 1992, Flexural ridges, trenches, and outer rises around coronae on Venus, *J. Geophys. Res.*, **97**, 16,069-16.083.

Scott, D.W., 1979, On optimal and data-based histograms. *Biometrika* **66**, 3.

Sheskin, D.J., 1997, *Handbook of parametric and nonparametric statistical procedures*. CRC press, Inc., 719 pp.

Simmons, M., S.C. Solomon, and B.H. Hager, 1997, Localization of gravity and topography constraints on the tectonics and mantle dynamics of Venus, *Geophys. J. Int.* **131**, 24-44.

Smrekar, S. E., 1994, Evidence for active hotspots on Venus from analysis of Magellan gravity data. *Icarus* **112**, 2-26.

Smrekar, S.E., and E.M. Parmentier, 1996, The interaction of mantle plumes with surface thermal and chemical boundary layers: Applications to hotspots on Venus. *J. Geophys. Res.* **101**, 5397-5410.

Smrekar, S.E., and Stofan, E.R., 1997, Corona Formation and Heat Loss on Venus by Coupled Upwelling and Delamination, *Science*, **277**, 1289-1294.

Smrekar, S.E. and E.R. Stofan, 2002, The gravity signature of Type 2 coronae on Venus and implications for corona formation mechanisms and structure of the lithosphere, *sub judice*.

Smrekar, S.E., E.R. Stofan, W.S. Kiefer, 1997, Large volcanic rises on Venus, in *Venus II*, eds. S.W. Brougher, D.M. Hunten, and R.J. Phillips, Univ. of Arizona Press, Tucson, pp. 845-878.

Smrekar, S. E., R. L. Comstock, and F.S. Anderson, 2002, A gravity survey of venusian coronae using cartesian and wavelet methods, *sub judice*.

Squyres, S.W., Janes, D.M., Baer, G., Bindschadler, D.L., Schubert, G., Sharpton, V.L., and Stofan, E.R., 1992, The Morphology and Evolution of Coronae on Venus, *J. Geophys. Res.*, **97**, 13611-13634.

Stofan, E.R., D.L. Bindschadler, J.W. Head, and E.M. Parmentier, 1991, Corona structures on Venus: Models of origin, *J. Geophys. Res.*, **96**, 20933-20,946.

Stofan, E.R. Stofan, E.R., V.L. Sharpton, G. Schubert, G. Baer, D.L. Bindschadler, D.M. Janes, and S.W. Squyres, 1992, Global distribution and characteristics of coronae and related features on Venus: Implications for the origin and relation to mantle processes. *J. Geophys. Res.* **97**, 13,347-13,378.

Stofan, E. R., S. E. Smrekar, D. L. Bindschadler, and D. A. Senske, 1995, Large topographic rises on Venus: implications for mantle upwelling. *J. Geophys. Res.* **100**, 23,317-23,327.

Table 1. Summary Statistics

Statistic	*Type 1*	*Type 2*	*Combined*
Count	406	107	513
Mean	256.8 km	236.8 km	252.6 km
Geometric Mean	220.7 km	208.0 km	218.0 km
Standard Deviation	150.9 km	127.8 km	146.5
Standardized Skewness	12.6	5.8	14.1
Standardized Kurtosis	12.7	4.1	14.2

Table 2. Type 1 Coronae

Topographic Group	*# of features*	*'best' # of bins*	*'best' answer*	*'best' + 1 bin*	*'best' – 1 bin*
TG1	30	6	accept	accept	accept
TG2	52	7	accept	accept	accept
TG3a	39	7	accept	reject	accept
TG3b	64	8	accept	reject	accept
TG4	111	8	accept	accept	accept
TG5	22	6	reject	accept	accept
TG6	5	4			
TG7	31	6	accept	accept	accept
TG8	39	7	accept	reject	accept
TG9	13	5	accept	accept	accept

Table 3. Type 2 Coronae

Topographic Group	*# of features*	*'best' # of bins*	*'best' answer*	*'best' + 1 bin*	*'best' – 1 bin*
TG1	0	-			
TG2	7	4			
TG3a	7	4			
TG3b	5	4			
TG4	25	6	accept	accept	accept
TG5	0	-			
TG6	0	-			
TG7	58	6	reject	accept	reject
TG8	4	4			
TG9	1	-			

Table 4. Results of ANOVA for overlapping 95% confidence intervals. Topographic groups are listed in order of increasing mean diameter.

Topographic Group	*LSD*	*Bonferroni*	*Scheffé*
TG8	X	X	X
TG9	X	XX	XXX
TG4	X	X	XX
TG1	X	XX	XXX
TG7	X	XX	XXX
TG2	XX	XX	XX
TG3b	X	X	X
TG3a	X	X	X
TG5	X	XX	X

Stofan, E.R., S.W. Tapper, J.E. Guest, P. Grinrod, and S. E. Smrekar, 2001, Preliminary analysis of an expanded corona database for Venus, *Geophys. Res. Lett.* **28**, 4267-4270.

Tapper, S.W., 1997, A Survey and Investigation of 'Stealth' Coronae on Venus: Distribution, Morphology, and Stratigraphy. *Lunar Planet. Sci. Conf. XXVIII.* abstract, 1415.

Figure Captions

Figure 1. Magellan radar image of a corona centered at 11.5°N latitude, 244°W longitude. The corona is a Type 1 corona with a raised rim and interior topographic high.

Figure 2. Empirical distributions of diameters for (a) Type 1 and (b) Type 2 coronae. Lognormal probability distributions are also shown for comparison.

Figure 3. Comparison of Type 1 and Type 2 geometric mean diameters with confidence intervals (see text for discussion). Overlap in confidence intervals indicates no statistical difference in the geometric mean values.

Figure 4. Illustration of relative frequency of occurrence for each topographic subgroup. Frequencies are shown for each corona type individually, as well as for the pooled data. The vertical axis indicates the number of coronae in each category.

Figure 5. Empirical distributions of corona diameters for Topographic Groups (a) 4 (Type 1), (b) 4 (Type 2), (c) 7 (Type 1), and (d) 7 (Type 2). All diameters have been transformed by taking the natural log.

Figure 6. Comparison of Type 1 and Type 2 geometric mean diameters with confidence intervals for Topographic Groups (a) 4 and (b) 7. Overlap in confidence intervals indicates no statistical difference in the geometric mean values.

Figure 7. Empirical distributions of combined Type 1 and 2 corona diameters for Topographic Groups (a) 1, (b) 2, (c) 3a, (d) 3b, (e) 4, (f) 5, (g) 6, (h) 7, (i) 8, and (j) 9. All diameters have been transformed by taking the natural log.

Figure 8. Results of ANOVA for topographic groups. Figure illustrates the geometric mean diameter and 95% Bonferroni interval for each subgroup (Type 1 and Type 2 coronae have been combined for this analysis). The topographic groups fall into two distinct diameter ranges, with group 7 transitional between the two.

Figure 9. Illustration of the frequency of occurrence for each topographic subgroup by geologic setting. Frequency distributions are shown for Type 1 and Type 2 coronae where the vertical axes indicate (a) the number of coronae in each category and (b) the relative occurrence of the topographic groups within each geologic setting.

Figure 10. Illustration of the frequency of occurrence for each topographic subgroup by geologic setting. Frequency distributions are shown for (a) Type 1 and (b) Type 2. The vertical axis indicate the number of coronae in each category.

Figure 11. Results of ANOVA for geologic settings. Figure illustrates the geometric mean diameter and 95% Bonferroni interval for each setting (Type 1 and Type 2 coronae have been combined for this analysis).

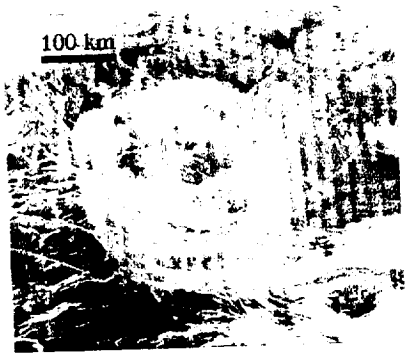
100 km

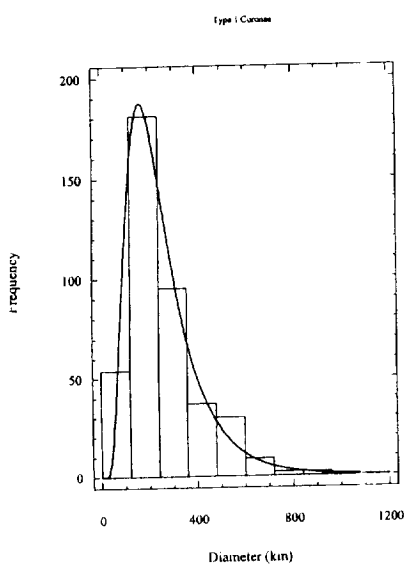
Type 1 Coronae
Frequency
200
150
100
50
0
0
400
800
1200
Diameter (km)

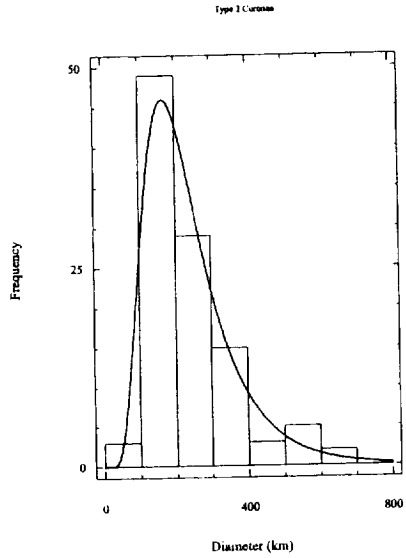
Type 2 Coronae
Frequency
50
25
0
0
400
800
Diameter (km)

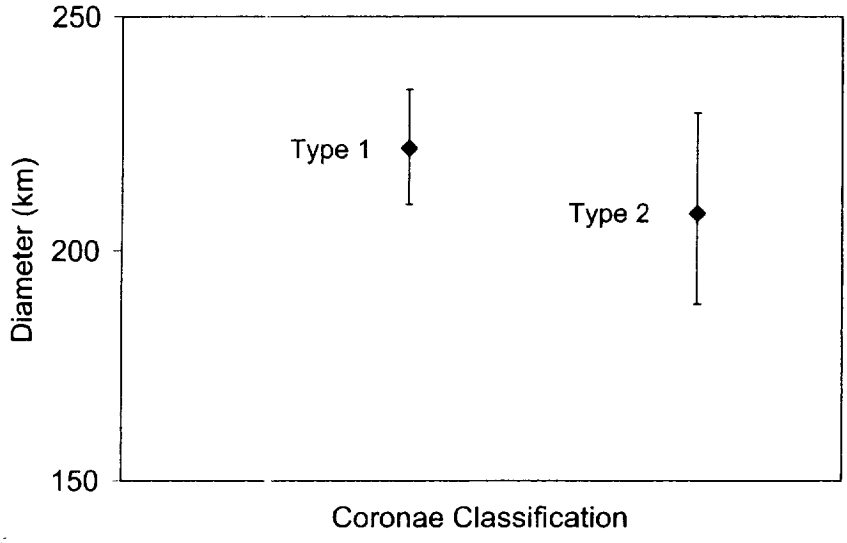
250
200
150
Diameter (km)
Type 1
Type 2
Coronae Classification

Figure 3

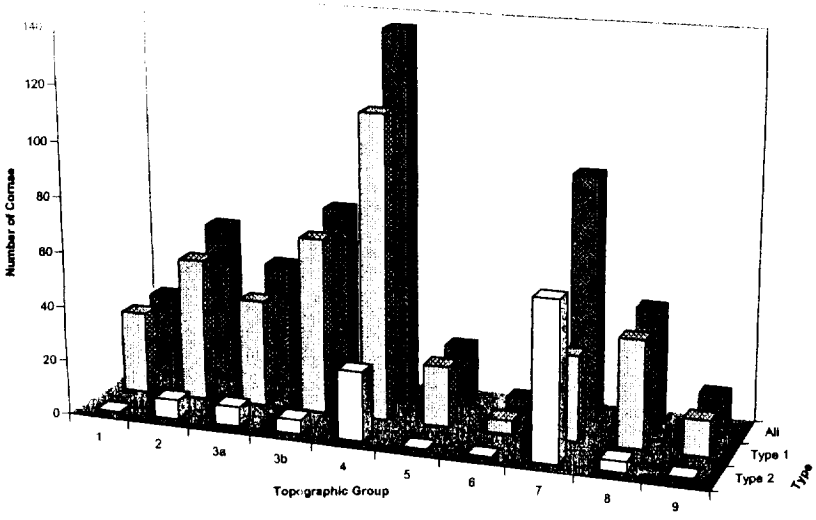
Number of Cornea
120
100
80
60
40
20
0
1
2
3a
3b
4
5
6
7
8
9
Topographic Group
All
Type 1
Type 2
Type

Figure 4

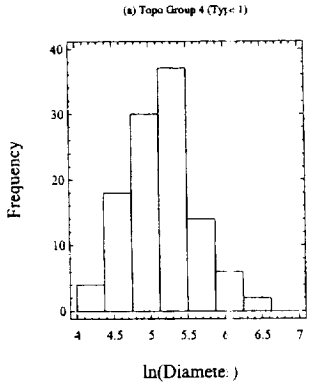
(a) Topo Group 4 (Type 1)
Frequency
40
30
20
10
0
4
4.5
5
5.5
6.5
7
ln(Diameter)

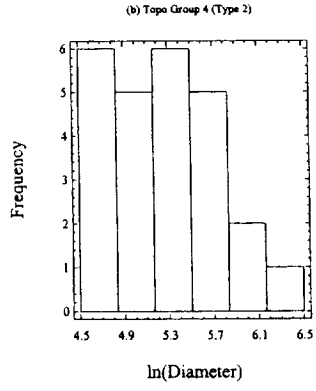
(b) Topo Group 4 (Type 2)
Frequency
6
5
4
3
2
1
0
4.5
4.9
5.3
5.7
6.1
6.5
ln(Diameter)

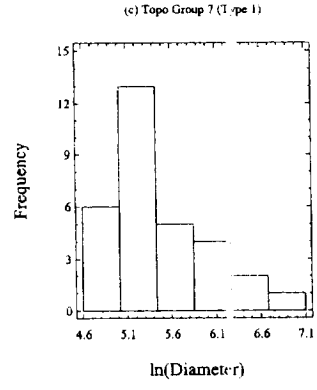
(c) Topo Group 7 (Type 1)
Frequency
15
12
9
6
3
0
4.6
5.1
5.6
6.1
6.6
7.1
ln(Diameter)

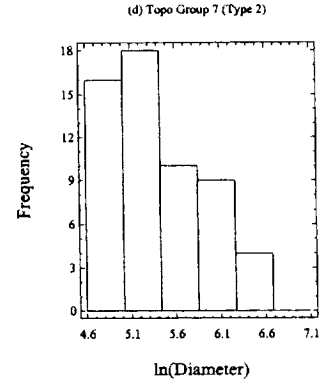
(d) Topo Group 7 (Type 2)
Frequency
18
15
12
9
6
3
0
4.6
5.1
5.6
6.1
6.6
7.1
ln(Diameter)

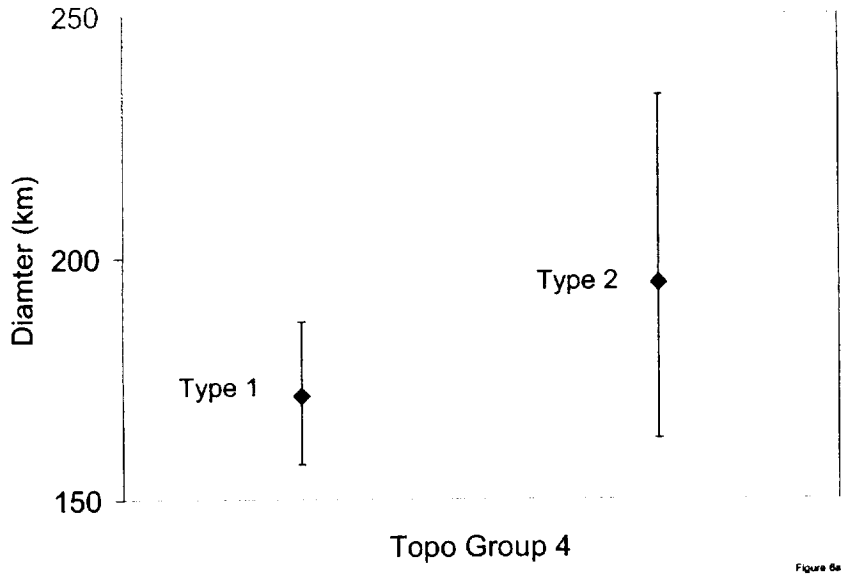

Figure 6a

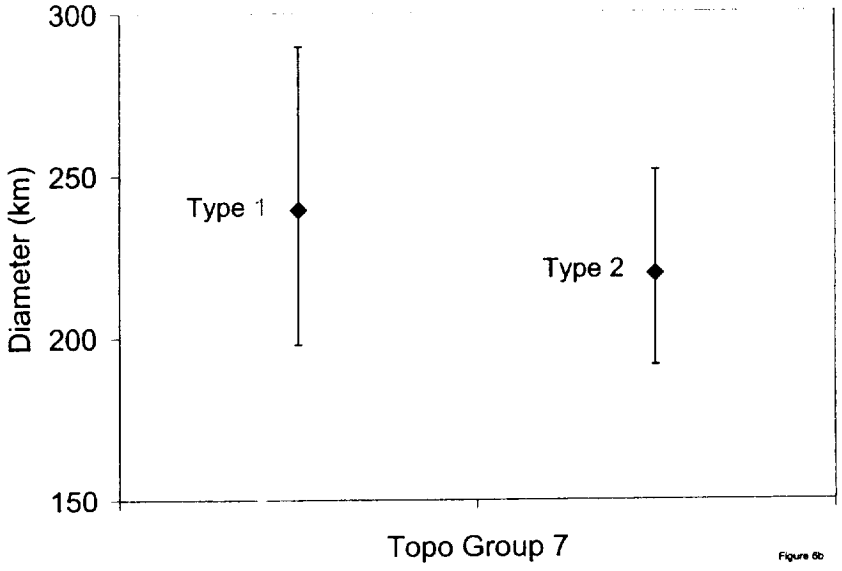

Figure 6b

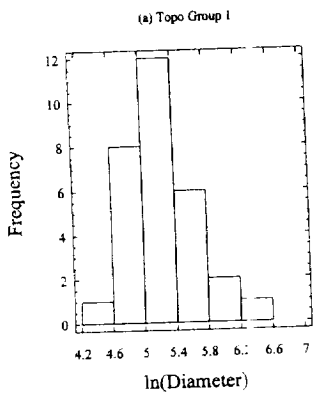

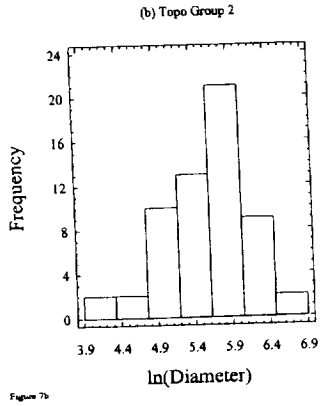

(c) Topo Group 3a

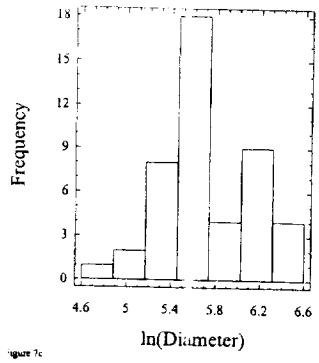

Figure 7c

(d) Topo Group 3b

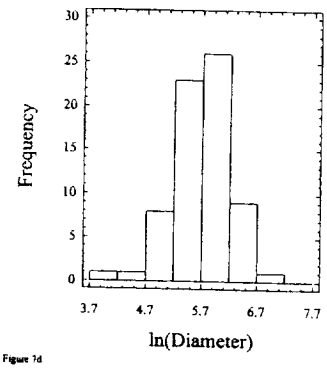

Figure 7d

(e) Topo Group 4

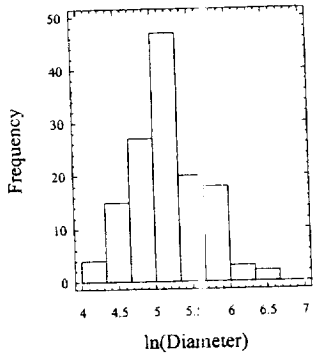

Figure 7e

(f) Topo Group 5

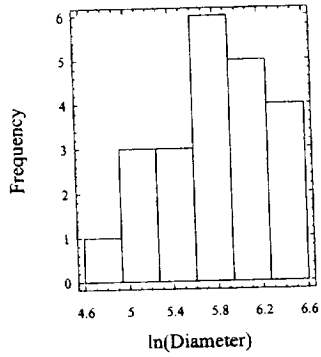

Figure 7f

(g) Topo Group 6

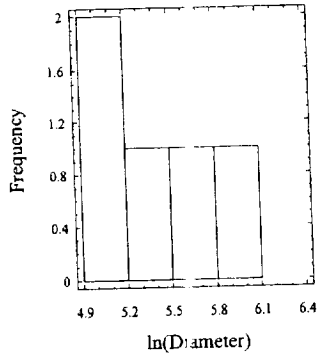

Figure 7g

(h) Topo Group 7

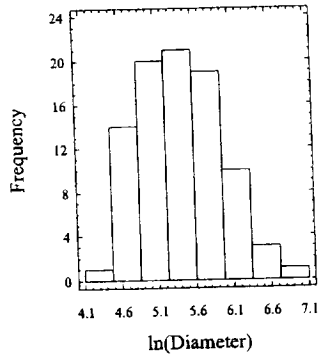

Figure 7h

(i) Topo Group 8

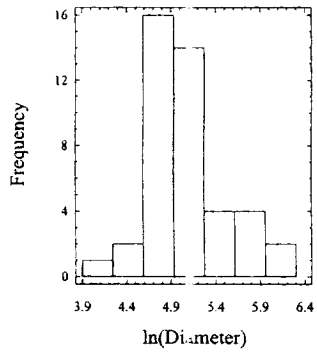

Figure 7i

(j) Topo Group 9

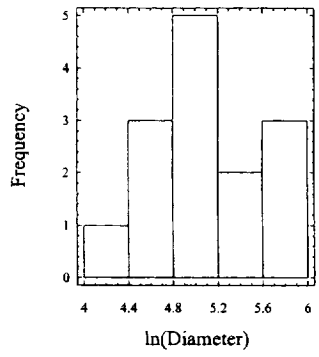

Figure 7j

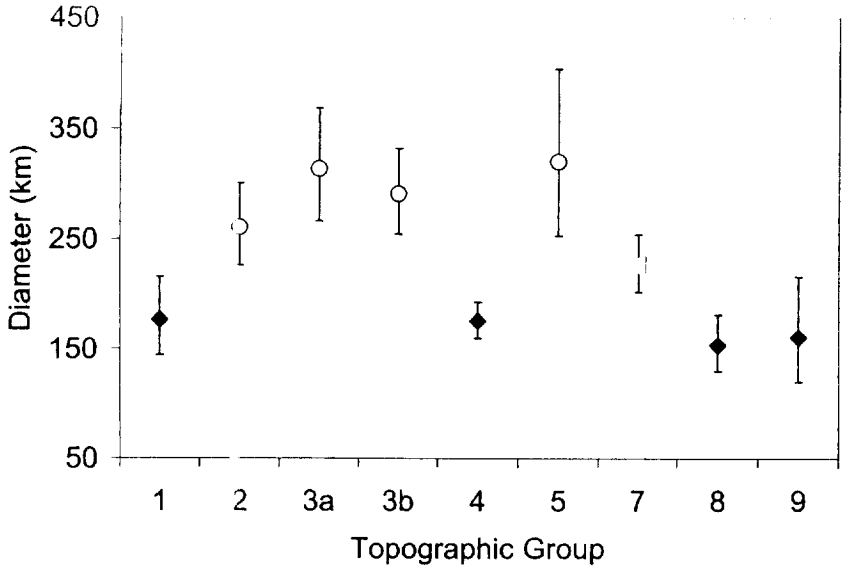

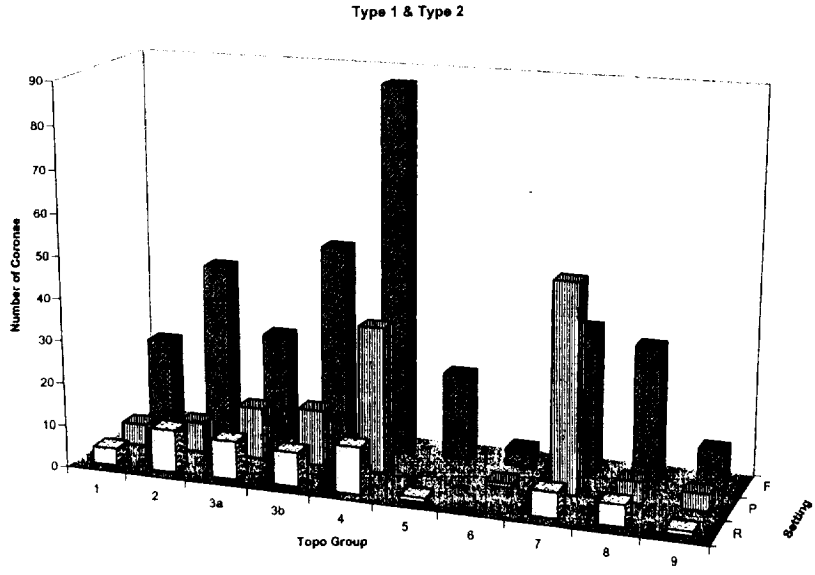

Figure 9a

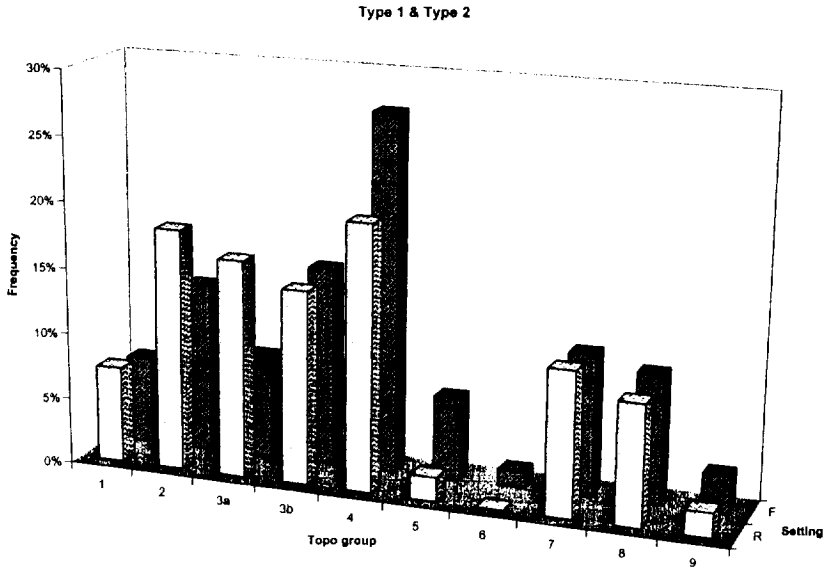

Figure 9b

Type 1

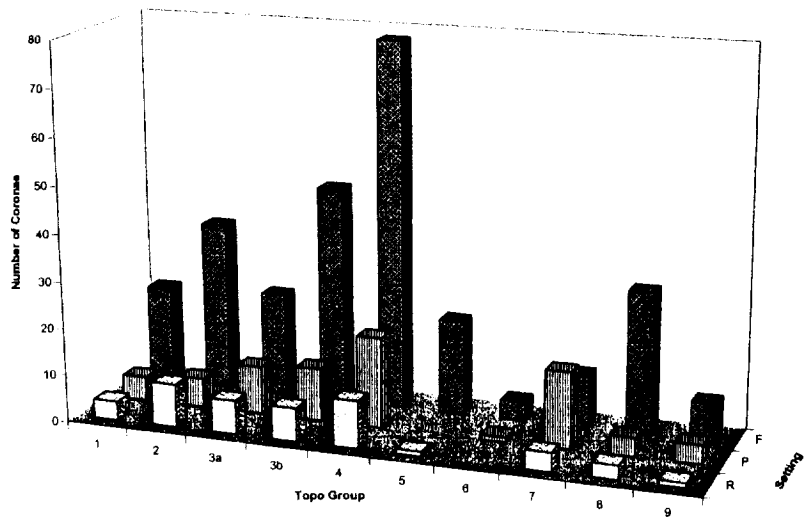

Figure 10a

Type 2

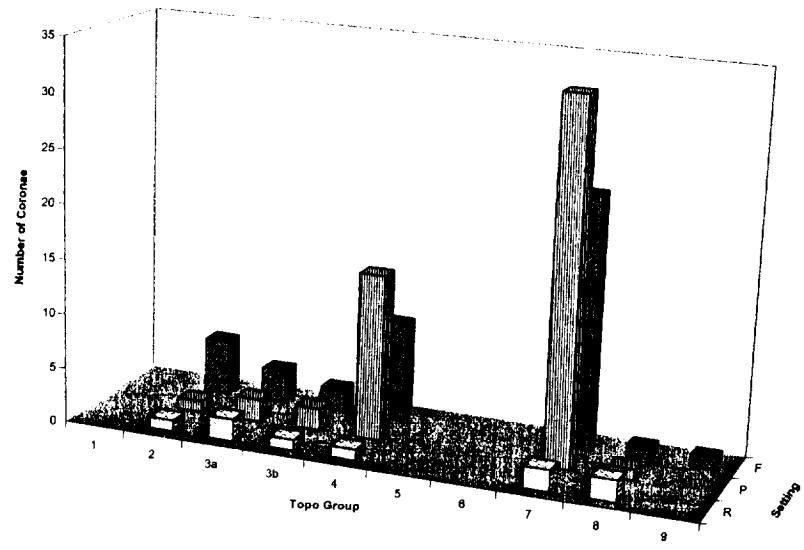

Figure 10b